

Voiding of ELSY Primary System During Steam Generator Leakage

M. Jeltsov, W. Villanueva, P. Kudinov

KTH Royal Institute of Technology, Stockholm, Sweden

E-mail contact of main author: marti@safety.sci.kth.se

Abstract. Harsh coolant environment in lead-cooled fast reactors (LFRs) can cause steam generator tube leakage and/or rupture (SGTL/R). Steam from secondary side can then be entrained by the primary coolant flow into the core which has adverse effects on the reactor performance including heat transfer deterioration and reactivity feedbacks. In this paper, this issue is studied using a deterministic-probabilistic approach.

Deterministic Eulerian-Lagrangian CFD model is used to simulate the primary coolant flow field of ELSY reactor and the post-SGTL transport of bubbles. Uncertainties in the relevant bubble size distribution and drag coefficient for bubbles moving in liquid metals have been studied. Probabilistic methodology to estimate the core and primary system voiding rates is proposed and demonstrated.

It has been found that a correlation by Tomiyama et al. (1998) gives the best prediction of drag for steam bubbles in liquid lead. Highest probability for being entrained by the flow is for small bubbles in contaminated coolant. The lower the leak in the SG, the higher the risk of void accumulation in the primary system. Analysis also revealed that certain amount of gas can stay entrapped in the primary coolant flow.

Key Words: LFR, CFD, Steam generator tube rupture/leakage, Bubble transport.

1. Introduction

1.1. Background

The Generation IV International Forum (GIF) aims to develop advanced nuclear power plants that can be licensed, constructed and operated in sustainable, economic, safe, reliable and secure manner. GIF selected six reactor types, so-called Generation IV reactors, as promising and worthy of further development. One of them is a lead-cooled fast reactor (LFR) [1].

Lead and lead-alloy coolants feature several attractive properties including low neutron capture, leakage, and moderation; high heat capacity, high boiling point, high thermal conductivity, high thermal expansion; chemical inertness with water and air [2]–[4]. This supports passive safety system designs with radiation shielding, natural convection and low system pressure [5], [6]. An overview of recent advancements, current status and future R&D needs regarding experimental and industrial LFR projects can be found in [4], [7], [8].

A fine balance between economics and safety of LFRs lies on assuring the feasibility of having all important reactor components (e.g. core, pumps, steam generators (SGs)) in the primary circuit, thus eliminating the need for, and economic burden of, an intermediate circuit which is used in sodium-cooled fast reactors (SFRs). However, complex thermal-hydraulic phenomena, severe operating conditions in terms of pronounced corrosion and erosion, large primary/secondary pressure differential and the SG proximity to the core raises safety concerns related to steam generator tube leakage and/or rupture (SGTL/R) [6], [9]. High uncertainty in the characteristics and statistics of the SG tube degradation and failures exists in LFRs due to lack of research and operational experience.

Leakage of SG tubes is not a new safety issue. PWRs have been plagued with SG reliability problems since the inauguration of the commercial technology in the late 1950's [10], [11]. By mid-1990's, about 50 % of the operating PWRs all over the world have had to remove from operation or repair more than 100,000 SG tubes indicating that there is a significant number of PWRs operating with defective SG tubes. Moreover, leaking SG tubes are even allowed up to a certain extent. US NRC limit for leakage through a single SG is about 0.4 L/min during normal operation and 3.8 L/min in case of accident [12]. Estimated frequency of a large rupture is about $6E-3$ /reactor year and about $6E-2$ /reactor year for a small leak [9]. SGs have also proven to be troublesome components in SFRs [13]. Only few studies in the literature address the SGTL/R issue in LFRs [14]–[16]. And it seems that most of the research attention has been paid on the rupture scenarios which may be thought to carry more risk compared to leakage.

A comprehensive review of SGTL/R phenomena and an approach to resolve the issue on risk analysis basis is described in [9]. Considering relatively harsher environment compared to LWRs and SFRs, there is no evidence to expect lower probability of SG leaks in LFRs. Moreover, it is difficult to detect the small leaks (characterized by longer incubation periods) in LFRs due to the opacity of the coolant.

1.2. Consequences of steam generator tube failure

In order to provide adequate defense-in-depth methods against the risks related to SGTL/R, relevant probabilities and consequences need to be clarified. The safety related phenomena and specific consequences have been identified hereafter.

- *Fluid-Structure Interaction (FSI)*. Sudden rupture of one or more SG tubes causes water from the high-pressure secondary side to burst into high-temperature/low-pressure primary side where it evaporates and expands rapidly leading to a sudden increase of primary system pressure [16]–[18]. The related hydrodynamic forces and sloshing may lead to FSI within the SG, between adjacent SGs and even in the reactor core.
- *Thermal-hydraulic coolant-coolant interaction (CCI)*. In certain circumstances, rapid transfer of energy from hot lead to cooling water can lead to steam explosion and/or sloshing [19]. Thermal CCI may result in local lead freezing due to overcooling by the feed-water which can cause flow blockage and/or deterioration of heat transfer.
- *Chemical CCI*. Oxide formation, precipitation and accumulation between water and lead may cause flow blockage and heat transfer deterioration in the core or in SGs. This phenomenon was the reason for core damage in a nuclear submarine Project 645 in 1968 in Soviet Union [20].
- *Radioactivity release to the environment*. Design pressures in primary vessel and containment in fast reactors are generally lower than that of the LWRs [13]. Pressure in the primary system increases due to excess water/steam from an SGTL/R that may call for venting. This can potentially release radioactive materials into the atmosphere.
- *Core voiding*. Hardened neutron spectrum and increased reactivity, especially in the active part of large cores, leads to positive coolant expansion/void coefficients fast reactors [21]–[25]. Entrainment of water vapor into the core region effectively reduces the coolant density or in an extreme case, voids the whole core leading to power excursions and reactivity initiated accidents (RIA) [26], [27]. Increased power and reduced heat transfer results in increased fuel and cladding temperature posing a threat of damage due to local burnout. The core voiding can take different forms as explained in FIG. 1. Scenario (a) is the build-up of small bubbles circulating in the primary system,

scenario (b) considers steam bubbles getting stuck in the in-core structures and scenario (c) can be envisaged as accumulation and growth of bubbles somewhere in the primary system where they then move to the core region in the form of a bigger slug. The effects of these scenarios on neutronics including detectability have been studied in [28], [29].

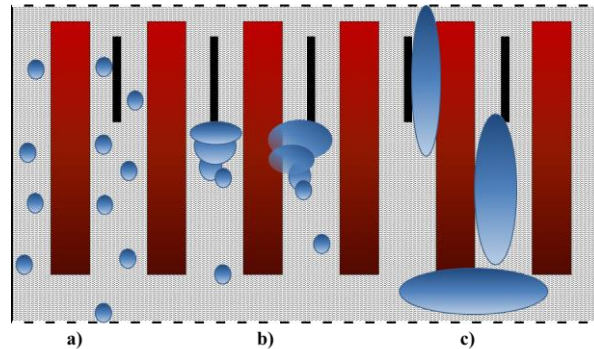


FIG. 1. Core voiding scenarios: Homogeneous voiding (a), void accumulation in the core (b) and slugs of void entering the core at once (c).

1.3.Outline

Considering the uncertainty and severity of potential consequences (e.g. core damage, release of radioactive material), SGTL/R accident can become a showstopper for licensing the LFR technology. According to the safety approach for the LFR plants developed within LEADER project, SGTL/R is classified as a DBC3 (design basis category 3) event which may occur very infrequently ($10^{-2} < f < 10^{-4}$) per reactor year and which the plant shall cope with within the defined radiological protection requirements [30].

The goal of this work is to quantify the likelihood and magnitude of primary system voiding during an SG tube leak in ELSY reactor. A methodology used to evaluate the primary system voiding is proposed. Aleatory (statistical) and epistemic (systematic) uncertainties pertaining to SGTL/R will be discussed and addressed. The drag model validation and use in the bubble transport simulations in the ELSY nominal operation primary system flow field is described.

2. Modeling of ELSY primary system

2.1.ELSY design

ELSY is a conceptual design of an industrial size LFR using simple engineering features while fully complying with the Generation IV goals [31], [32]. It has thermal power of 1500 MW with electric design power of 600 MW (at efficiency of ~40%).

ELSY is a pool-type reactor with all important components placed inside the cylindrical vessel with hemispherical bottom (FIG. 2 (left)). The height and diameter of the reactor are 8.65 m and 12.3 m, respectively. Reactor roof is a steel plate with penetrations for several in-pool components (e.g. fuel assemblies, SGs and dip coolers). In normal operation, the heat produced in the core is removed by eight compact spiral-wound tube bank SGs [33] (FIG. 2 (right)). SGs are anchored to the roof by a flange and immersed in the primary coolant as symmetrically positioned pairs around the core. The core is in the lower middle-part of the primary system to enhance the natural circulation heat removal capability. Coaxial pumps installed in every SG unit drive circulation of liquid lead.

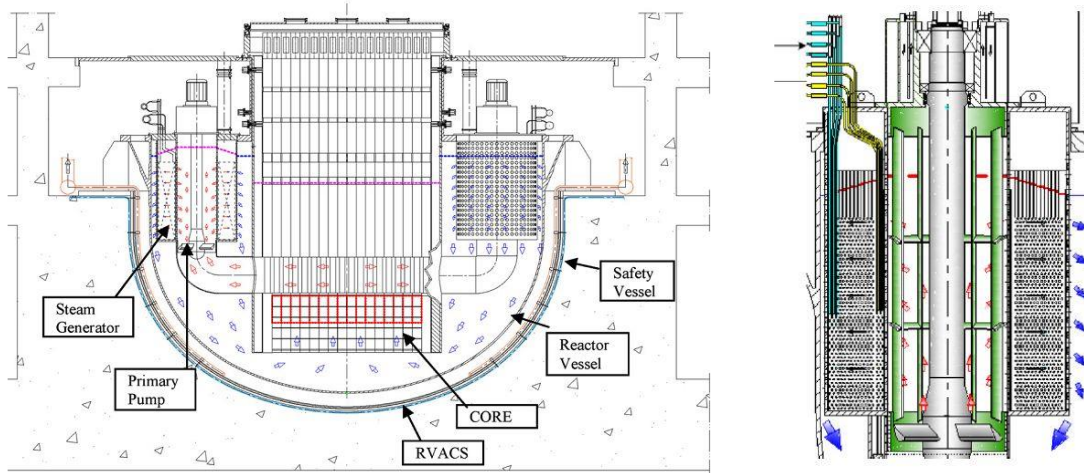


FIG. 2. Primary system configuration of ELSY (left) and spiral-wound SG (right).

The primary side of ELSY is characterized by relatively slow (<2 m/s) single-phase liquid metal flow at hydrostatic pressure and high temperature (in the range of 400 - 480°C). Secondary side operates at high flow rates and high pressures (13 - 26 MPa) using either Rankine (steam) or Brayton (gas) cycle depending on the particular choice [34].

2.2. Simulation of nominal steady state operation conditions

Lead flow field in the primary system of ELSY at nominal operational conditions is simulated with Star-CCM+ CFD code. Computational domain represents a $1/8^{\text{th}}$ slice of the reactor and its components including reactor core, SG and a 90 degree bent connection pipe (see FIG. 3).

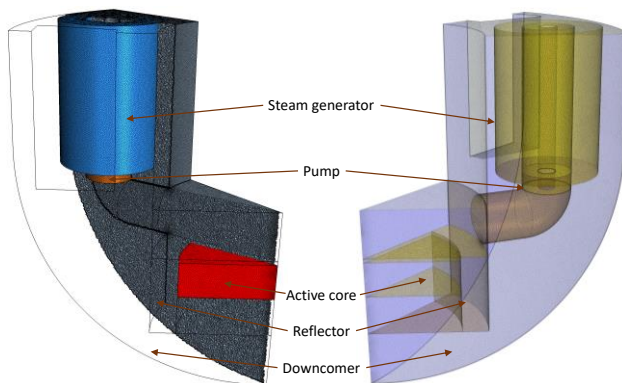


FIG. 3. Mesh and definition of regions in ELSY computational domain

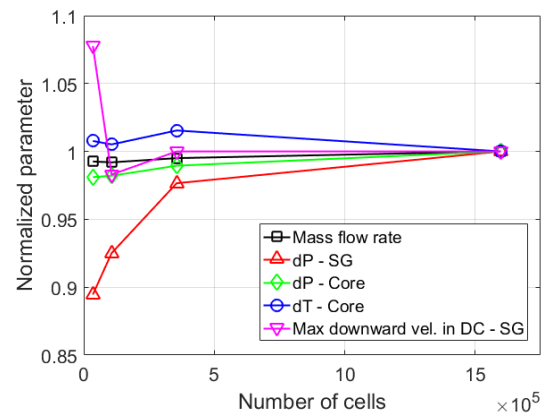


FIG. 4. Mesh study results. Parameters normalized by their finest mesh value.

The steady state incompressible turbulent flow of liquid lead under gravity is simulated using a coupled implicit solver with 2^{nd} -order upwind discretization scheme. Lead material properties are defined according to lead/LBE handbook prepared by OECD/NEA [4]. Reynolds-Averaged Navier-Stokes (RANS) formulation in Eulerian framework with Realizable $k - \varepsilon$ eddy viscosity turbulence model is selected for momentum and energy transfer. A Buoyancy Driven Two-Layer All- y^+ wall treatment is used, in which the model automatically switches between resolving viscous sublayer in fine mesh regions and uses wall functions in coarser regions [35]. The core, reflector, pump and SG are modeled as porous media using inertial resistance coefficients to predict the pressure drops in those regions. Core power is defined as total heat source of 187.5 MW ($1/8^{\text{th}}$ of 1500 MW). Heat removal in the SG is modelled by a temperature dependent heat sink that removes 187.5 MW when lead is at 480°C and 0 W when lead is at

335°C, the temperature of the water at the secondary side inlet. Flow is driven by a momentum source defined in the pump.

A mesh study was carried out to assess the effects of numerical discretization on the relevant physical parameters (see FIG. 4). A model with ~356,000 polyhedral cells and 8 prismatic layers on the wall was selected. This model predicted the mass flow rate of 16,090 tons/s and core inlet and outlet temperature of 402.6 °C and 480.8 °C, respectively. Pressure drop over the core was 0.94 bar and over the SG 0.42 bar. These are in accordance with the design values [32], [36], [37]. Steady state temperature and velocity fields are shown in FIG. 5. The separation of hot and cold leg as well as lead heat-up in the core and cool-down in the SG are clearly visible in the temperature plot. Highest velocity is detected in the inner curve of the bend and in the pump where the flow area is smallest. Velocity in the downcomer, an important parameter for bubble transport, is ~0.26 m/s on average whereas maximum downward component is 0.53 m/s.

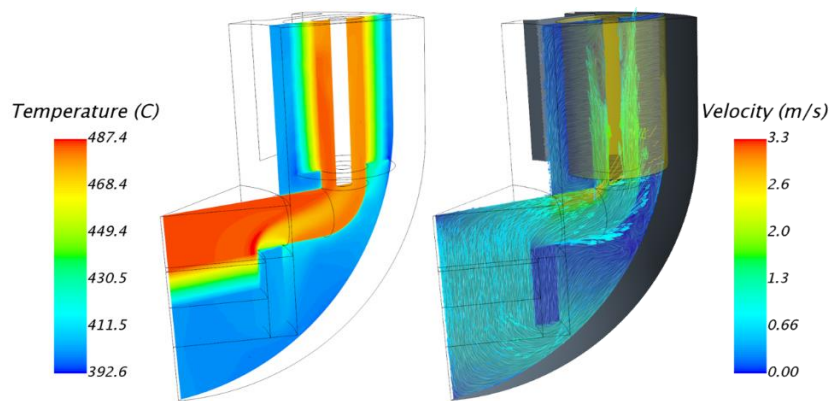


FIG. 5. ELSY steady state temperature and velocity fields.

3. Bubble transport phenomena in liquid lead

Formation, motion, coalescence and break-up are the fundamental hydrodynamic phenomena governing bubbly flows [38]. These phenomena depend on the physicochemical properties of the gas and liquid phases and thermal-hydraulic state of the system in order to determine, among others, the interface morphology and the bubble size distribution. Successful simulation of most engineering applications involving bubbles, drops and/or particles relies on the accuracy of size distribution together with empirical models for size-dependent mass/momentum/heat transport characteristics. In this chapter, we attempt to characterize the bubble size distribution during an SGTL in liquid metal reactors using experimental data from literature. Secondly, we address the uncertainty in the drag coefficient for gas bubbles in liquid lead.

3.1. Bubble size distribution

The maximum stable bubble size is governed by the hydrodynamic instabilities on the gas-liquid interface above which the bubble is subjected to break-up. When the forces on the liquid side exceed the surface tension of the gas-liquid interface the bubble becomes unstable and disintegrates [39], [40]. Break-up occurs at critical Weber number which depends on the type of deformation and on the flow pattern around the bubble [41]. Estimates for critical Weber number at different bubble-liquid configurations may vary from 1 to 5 [41], [42]. The maximum diameter that corresponds to this upper limit of critical Weber number is 5.3 mm.

Bubble size distribution has been measured at LFR-relevant conditions in few studies (see FIG. 6).

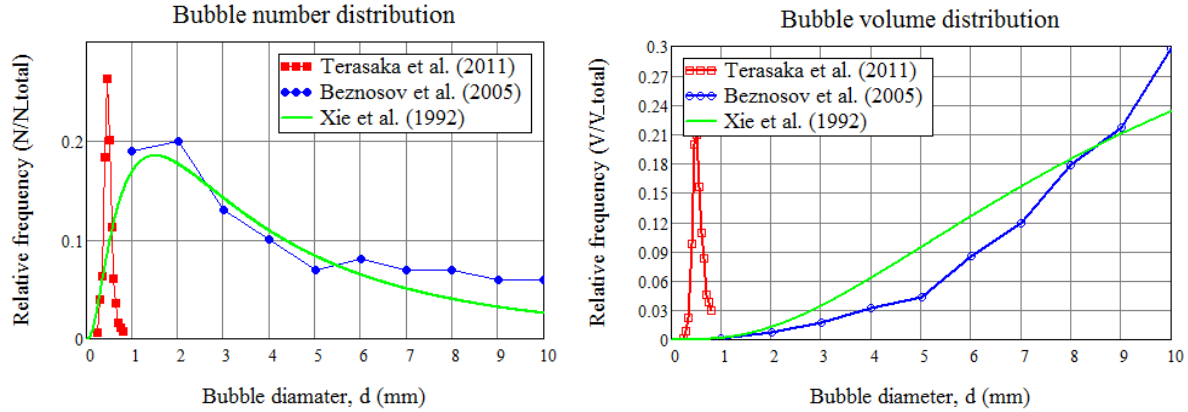


FIG. 6. Number and volume distributions of experimentally observed bubbles.

Terasaka et al. measured size distribution of nitrogen bubbles generated through a 15 μm slit orifice submerged in water at normal conditions [43]. Pressure drop over the nozzle was 1 bar. This small crack resembles an early-phase SG tube failure and produces “submilli-bubbles” with a mean diameter of 0.499 mm. Beznosov et al. performed experiments of bubbling 150-250°C water-steam mixture at 22-24 MPa into liquid lead at a depth of 2 m through a 1 mm nozzle and observed a range of 1-10 mm bubbles [44]. Xie et al. blew gas bubbles (mostly nitrogen, but also argon and helium) into 100°C molten Wood’s metal and proposed a log-normal bubble size distribution [45].

Considering that the slit-like cracking leading to small, infrequent bubbles, is the most common type of tube failure, the smaller end of bubble size spectrum is of high interest. Bubbles leaking in small cracks can be “wiped away” by turbulent flow before reaching full equilibrium size. Smaller bubbles are also more prone to be entrained by the flow compared to large, buoyant bubbles. Based on this, a range of 0.1–10 mm has been used here.

3.2. Drag coefficient

Bubble rise in liquid is a function of bubble characteristics (size and shape), properties of the gas-liquid system (density, viscosity, surface tension, concentration of impurities), liquid motion (velocity, turbulence), and system state (pressure, temperature, gravity, gradients) [38]. Accurate prediction of single bubble motion requires definition of a complete set of forces involved. According to the Newton’s second law applied to a bubble:

$$\Sigma \mathbf{F} = \mathbf{F}_B + \mathbf{F}_W + \mathbf{F}_D = m\mathbf{a} \quad (1)$$

where the buoyancy force \mathbf{F}_B is defined as the weight of fluid displaced by the object,

$$\mathbf{F}_B = V_G \rho_L \mathbf{g} \quad (2)$$

the weight \mathbf{F}_W is a force acting on an object due to gravity,

$$\mathbf{F}_W = V_G \rho_G \mathbf{g} \quad (3)$$

and the drag force \mathbf{F}_D is an approximation of the combined effect of different forces (surface tension, viscous shear etc.) acting in the direction of the surrounding flow:

$$\mathbf{F}_D = \frac{1}{2} \rho_L |\mathbf{U}| \mathbf{U} C_D A_e \quad (4)$$

When the buoyancy force exceeds the weight objects tend to rise. This, also called as positive buoyancy, is the case for gas bubbles in liquids. When the drag force, exerted on the object by the flow, dominates the object is entrained. When all forces are at equilibrium, bubble moves at a constant, so-called terminal rise velocity:

$$U_T = \sqrt{\frac{4(\rho_L - \rho_G)gd_e}{3\rho_L C_D}} \quad (5)$$

The drag coefficient, C_D , is a dimensionless quantity describing the resistance of a bubble in fluid flow. In practice, it is difficult to adequately resolve the complex small-scale phenomena responsible for the drag. Therefore, empirical correlations have been developed to establish a relationship between bubble morphology, flow conditions and drag [38].

Jamialahmadi et al. developed a correlation for the terminal rise velocity applicable in a wide range of gas-liquid properties by combining the Stokes' law describing steady creeping flow past small spherical particles with no slip condition (U_T^{sp}) and Mendelson's equation based on wave analogy (U_T^w) [39], [46], [47]:

$$U_T = \frac{U_T^{sp} U_T^w}{\sqrt{(U_T^{sp})^2 + (U_T^w)^2}} \quad (6)$$

Very few experiments have been done for gas bubbles rising in liquid metals and none have been found for lead alloys. However, there are few experiments with other liquid metal systems. In FIG. 7, the prediction of Eq. 6 is compared with relevant experimental data for rising bubbles found in literature: argon in mercury and in distilled water (to check the reliability of the measurement technique) [48], nitrogen in mercury [49], argon in tap water and in eutectic GaInSn [50]. It appears that Eq. 6 matches the experiments in water and mercury reasonably well, but overestimates the velocity in GaInSn. Latter is attributed to the impurities (e.g. oxides) in the melt reducing the surface tension and increasing drag [51]. Even though there is no data for bubbles smaller than 1 mm, the uncertainty in this region is considered small since the phenomena is well-described by Stokes' law [39]. From these considerations, it can be assumed that Eq. 6 predicts adequately terminal rise velocity of bubbles in liquid metals.

Eq. 6 is now used as a benchmark in the drag model validation. A model of $0.5 \times 0.5 \times 2$ m column of stagnant lead was set up in Star-CCM+. Bubbles of 0.1-10.0 mm in diameter were injected at the bottom of the column and their rise was simulated using a Lagrangian model with surface tension, drag and history force. Six empirical drag coefficient correlations were tested:

- Schiller-Naumann correlation. Suitable for spherical solid particles, liquid droplets, and small-diameter bubbles [52],
- Rodrigue correlation. An explicit drag correlation derived based on a correlation for terminal rise velocity of a single gas bubble in steady Newtonian fluids [53], [54],
- Bozzano and Dente correlation. This correlation accounts simultaneously for friction and shape deformations of bubbles [55], and
- Tomiyama et al. correlation. A correlation based on a force balance approach in combination with available theoretical and empirical data for terminal rise velocity [56]. Three versions of this correlation to cover a wide range of bubble-fluid systems:
 - pure system:

$$C_D = \max \left\{ \min \left[\frac{16}{Re_p} (1 + 0.15 Re_p^{0.687}), \frac{48}{Re_p} \right], \frac{8}{3} \frac{Eo}{Eo + 4} \right\} \quad (7)$$

- slightly contaminated system:

$$C_D = \max \left\{ \min \left[\frac{24}{Re_p} (1 + 0.15 Re_p^{0.687}), \frac{72}{Re_p} \right], \frac{8}{3} \frac{Eo}{Eo + 4} \right\} \quad (8)$$

- and contaminated system:

$$C_D = \max \left\{ \frac{24}{Re_p} (1 + 0.15 Re_p^{0.687}), \frac{8}{3} \frac{Eo}{Eo + 4} \right\} \quad (9)$$

FIG. 8 illustrates the variation in the results that is attributed to different assumptions in each model. Schiller-Naumann model, based on the Stokes law combined with a constant for inertial regime, fails to capture the non-linear medium-size bubble regime. Rodrigue correlation also fails to predict the rise velocity curve shape. Correlations by Tomiyama, and Bozzano and Dente successfully predict the general shape of the velocity curve. These correlations differ from others in that they take Eötvös number (Eo), a ratio of body forces to surface tension, into account. However, Tomiyama models predict the peak slightly better and are flexible in terms of modeling the effect of contamination level, which seems to be important. In order to cope with the uncertainty in drag model, two bounding correlations are used in the remainder of this work – the pure and contaminated by Tomiyama.

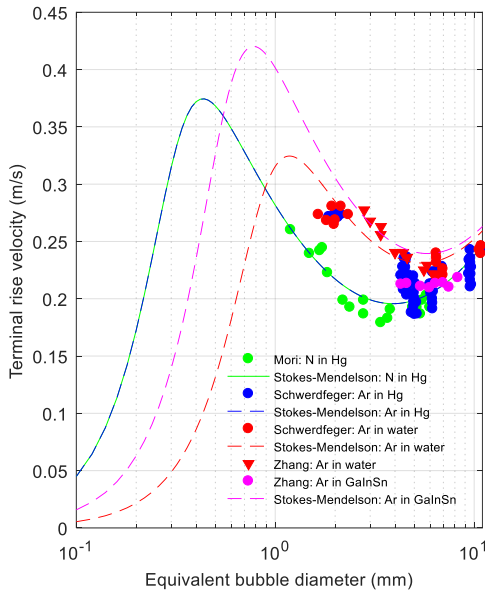


FIG. 7. Terminal rise velocity of different gas-liquid systems compared with Eq. 6.

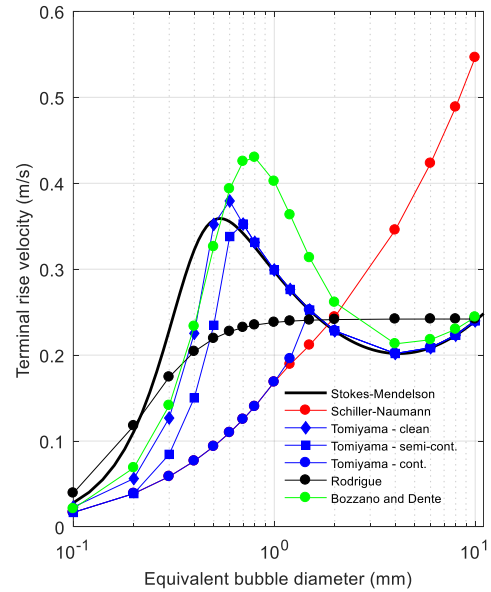


FIG. 8. Rise velocity of steam bubble in liquid Pb with different drag correlations.

4. LFR primary system voiding analysis

4.1. Methodology

Transport of steam bubbles in ELSY primary system is simulated with the verified CFD model and validated drag correlations. Primary system voiding characteristics are estimated by injecting, collecting and counting bubbles at different locations in the system. This allows to obtain the fraction of “dangerous” bubbles in all injected bubbles per injection location FIG. 9. P1-P3 are the probabilities that that bubbles injected at random position on the injector plane reach the monitoring location in the primary system (core inlet, pump inlet). E1-E3 are the probabilities that randomly injected bubbles escape from the system through lead free surface.

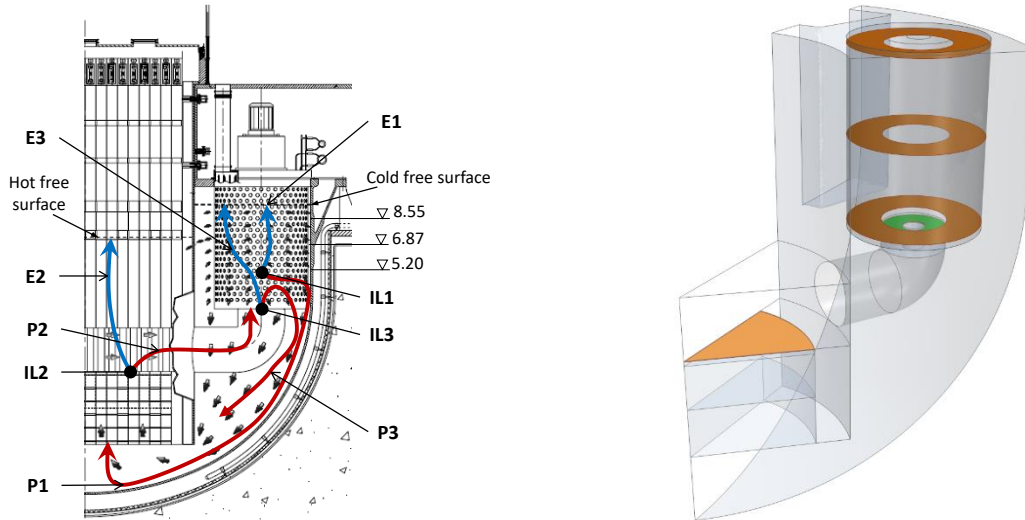


FIG. 9: : Injection locations (IL1-IL3, brown), entrapment (P1-P3) and escape probabilities (E1-E3).

Two definitions have been used for “dangerous” bubbles – i) bubbles that reach the location of interest inside the primary system and ii) bubbles that do not escape the primary system through free surface. Such distinction helps to determine the amount of bubbles accumulating in the primary coolant which can happen due to, for example, low-pressure recirculation zones.

The water/steam accumulation rate in the primary system is estimated as:

$$\dot{Q}_{primary} = \dot{Q}_{leakSG} \sum_{i=1}^N \left(f_{d_i} \prod_{j=1}^3 P_{j_{d_i}} \right) \quad (10)$$

where \dot{Q}_{leakSG} is the volumetric leak rate, f_{d_i} and $P_{j_{d_i}}$ are volume fractions and probabilities for a bubble with size d_i , and N is the number of bins in the bubble size distribution. P_i means either entrapment probability or one minus escape probability, depending which definition for dangerous bubbles is used.

It can be that in certain circumstances the bubbles that leak into primary system are entrained by the flow but do not manage to get through the core, meaning that the void builds up somewhere in or before core and can move to the core at once. This void accumulation is estimated using only the first probability (P1, or E1):

$$\dot{Q}_{core} = \dot{Q}_{leakSG} \sum_{i=1, N} f_{d_i} P_{1_{d_i}} \quad (11)$$

The gas carry-under factors (fraction of flow that is entrained) are evaluated to provide leak rate-independent characteristic for the gas entrapment:

$$CU_{core} = \frac{\dot{Q}_{core}}{\dot{Q}_{leakSG}}, \quad CU_{primary} = \frac{\dot{Q}_{primary}}{\dot{Q}_{leakSG}} \quad (12)$$

While the probabilities and bubble volume distributions are design specific (depend on e.g. coolant material, detailed geometry) the methodology is applicable for any LFR design.

4.2.ELSY primary system voiding results

Entrapment probabilities

The probability of “dangerous” as a function of bubble size is shown in FIG. 10. Clean system is represented by black and contaminated (realistic) system by red curves. Round symbols take only the bubbles reaching the monitor location into account (e.g. core inlet, pump inlet) while square symbols consider also the bubbles that do get stuck somewhere in the primary system. Injection location 1 (IL1) refers to the case where bubbles are transported from SG to core.

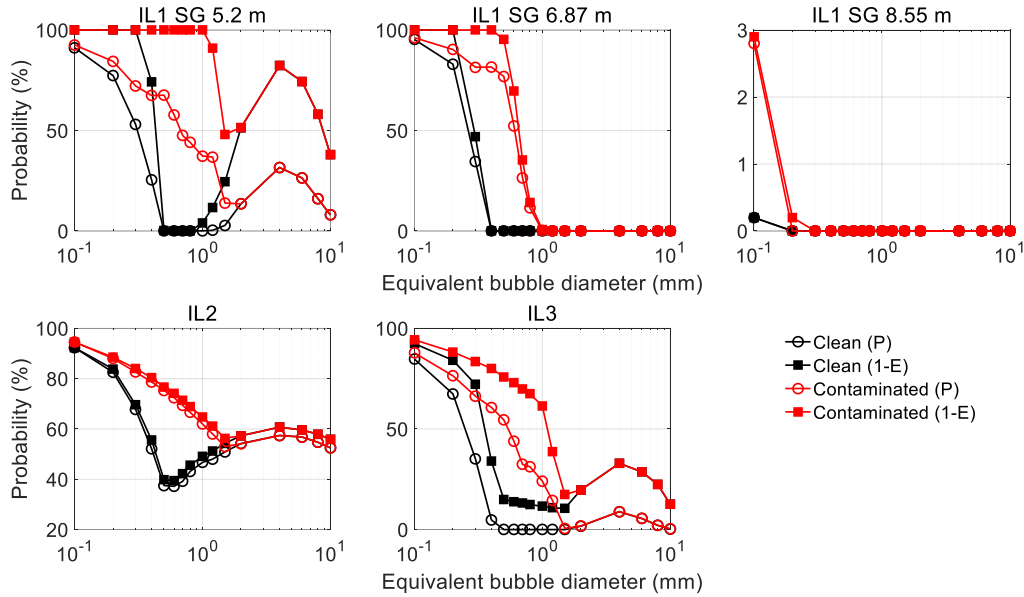


FIG. 10. Bubble entrainment probabilities.

Based on those results, following can be learned:

- All curves reflect the **non-linearity of the drag coefficient** as a function of bubble size, regardless the injection location. Sub-millimeter bubbles ($d_B < 0.5$ mm) are always entrained by the flow because of the maximum drag in viscosity dominated regime. Mid-size bubbles (0.5 mm $< d_B < 1.2$ mm) always have the lowest entrainment probabilities (surface tension regime with the lowest drag), which increases again for the larger bubbles ($d_B > 1.2$ mm) for which the form drag starts.
- **Effect of leak location.** Bubble entrainment probability increases with the depth of leak location in the SG. This is explained by more pronounced downward velocity component in the bottom of the SG region and adjacent to SG in the downcomer (FIG. 11).

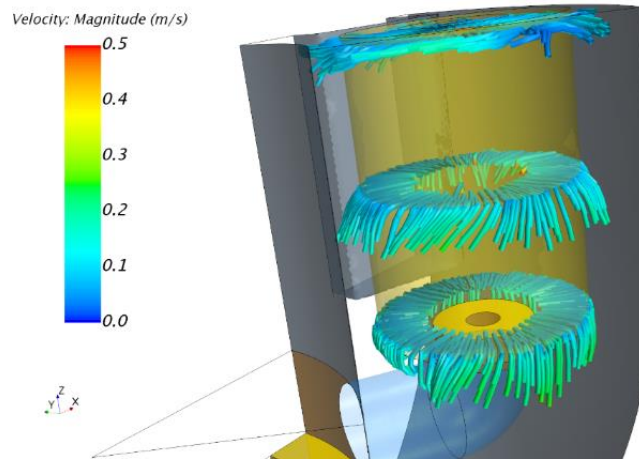


FIG. 11. Velocity streamlines originating from the three injection locations in the SG.

- **Effect of liquid contamination.** Contamination increases the entrainment probabilities due to increased drag. The effect is especially strong in the 0.2-2.0 mm range, which is so-called surface tension dominated since this property depends on the interface purity.
- **Effect of definition of “dangerous” bubbles.** Bubbles which do not escape the system nor reach the monitored location of interest, are assumed to remain in the system. This effect is governed by the balance between drag and buoyancy forces and is pronounced for mid-size bubbles (peak in the probability of remaining in FIG. 12). When either buoyancy or drag strongly dominates, e.g. low velocity region in the upper part of the SG or high velocity in the connecting pipe, respectively, bubbles do not remain in the flow. Therefore, the (1-E1) probability results in more conservative voiding analysis.

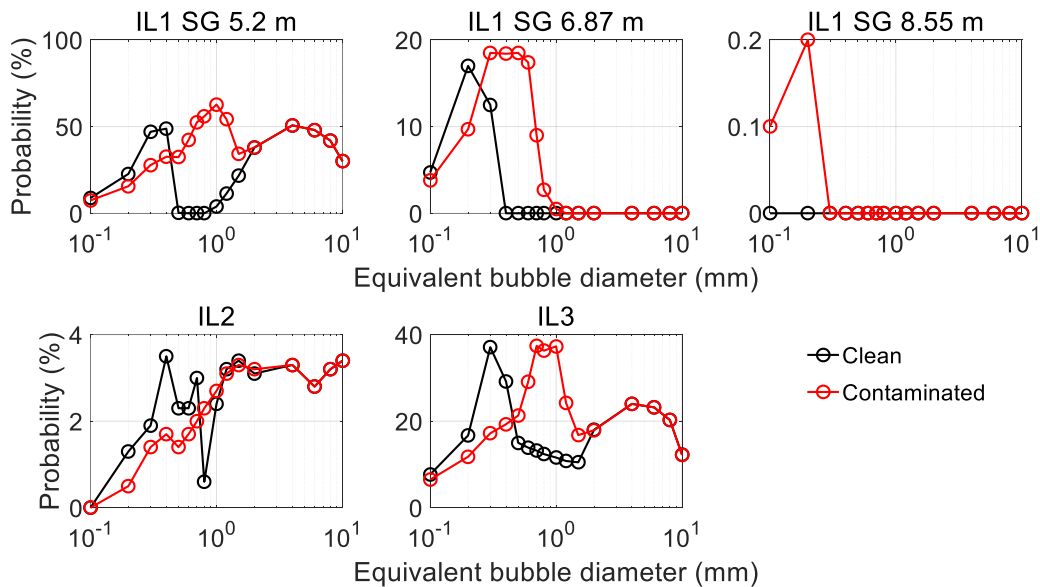


FIG. 12. Probability for bubbles to remain in the system.

Void accumulation rates

Experimental studies and SGTL/R accidents in PWRs have demonstrated leak rates from single bubble per minute up to 10 L/min ([13], [43], [44], [57]–[59]). This translates up to 15 m³/day which can be a concern even when a fraction of it reaches the core. Considering that since atmospheric primary side the pressure difference in LFRs is larger than that of PWRs, such leak rates are definitely of interest here too. FIG. 13 illustrates the void buildup rates in the primary system and in the core as a function of leak rate considering the entrainment probabilities calculated earlier. Different curves correspond to different bubble size distributions and system contamination levels. It is clear that in case of leak at the top of SG (8.55 m level), gas entrainment is negligible. When leak occurs in the middle of SG (6.87 m level), only small bubbles in contaminated system are entrained. It is instructive to note that such small size distribution results from small leak rates of up to 1 L/min that corresponds to void accumulation of 0.5 L/min in the core and 0.4 L/min in the primary system. The most dangerous leak location is the bottom region of SG (5.2 m level) where smallest bubbles contribute most to the void buildup, but also larger end of the size distribution is important.

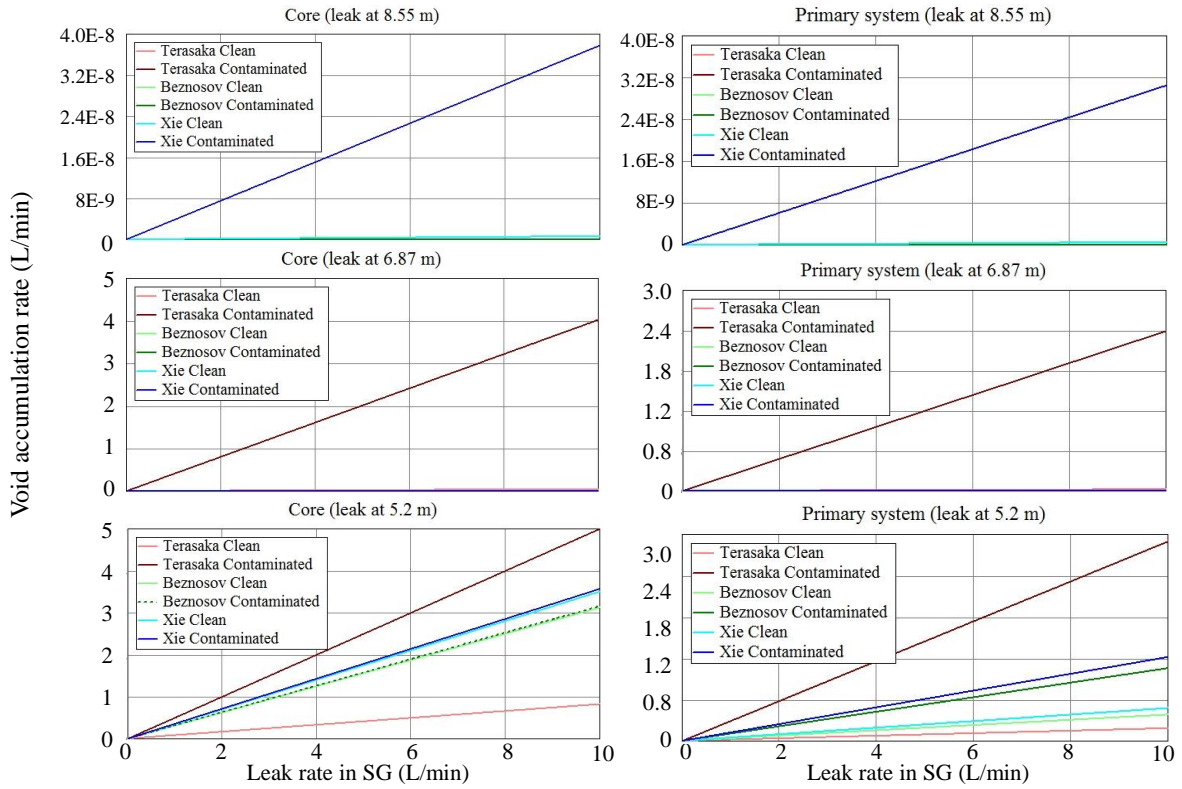


FIG. 13. Core and primary system voiding rates as a function of leak rate in SG.

FIG. 14 shows the carry under factors for different analyzed configurations. It can be seen that the most dangerous is a leak in the lower part of the SG and bubble entrainment is pronounced by small bubble sizes and contaminated systems. Up to 50% of the gas from leak can reach core.

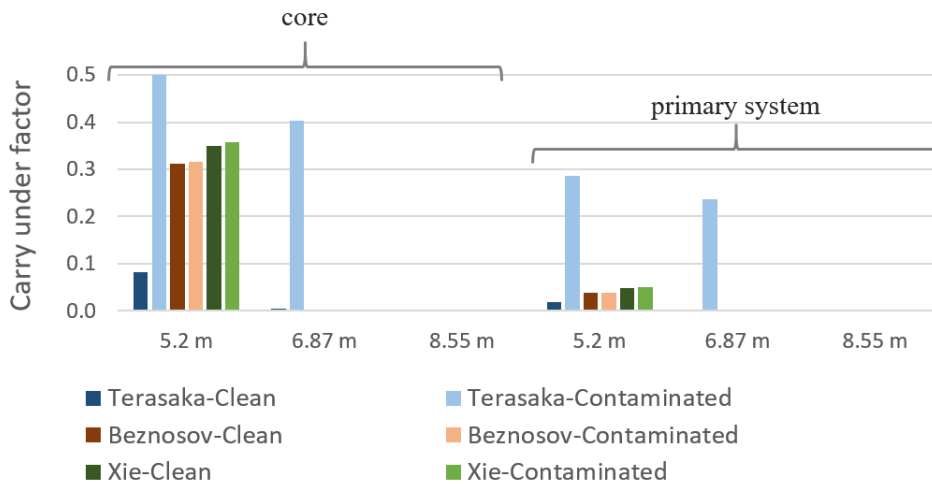


FIG. 14. Carry under factors.

5. Conclusions

Steam generator tube leakage is an important safety issue in LFRs due to potentially severe consequences on the reactor performance including reactivity-initiated accidents and heat transfer deterioration in the core. Since in many reactors the tubes have leaked before rupturing, this study focusses on the behavior of small discrete bubbles in the primary system of an LFR.

ELSY reactor has been used as a reference case. Bubble-coolant multiphase flow has been modelled with a Eulerian-Lagrangian CFD approach. A mesh study of the flow model has been carried out to verify the solution of the local velocity field which is important for drag modeling.

Several uncertain parameters governing the SGTL phenomena have been analyzed in detail. Among those, bubble size distribution and drag coefficient are found to be the most crucial and receive the main attention. Since slit-like cracking is the most common type of tube failure, the smaller end of bubble size spectrum (0.1-10 mm used here) is of high interest. Drag coefficient has been validated using the experimental data, though scarce, available for bubble motion in liquid metals.

A probabilistic-deterministic methodology has been proposed to quantify separately voiding of the core, primary system and identify fraction of bubbles that get stuck in the primary system.

The main outcome includes the following:

- Gas entrainment depends on the leak location, bubble size distribution and system contamination levels.
- Leak in the lower part of SG is the most dangerous in terms of subsequent gas entrainment.
- Gas leaking in the upper part dominantly escapes to the free surface of lead.
- Gas carry under is significant for small bubbles in contaminated systems which corresponds to increased drag situation.

6. Acknowledgements

The work was performed in the framework of 6th and 7th EU Framework Programme projects ELSY and LEADER, respectively. Authors are grateful to Dr. Johan Carlsson (JRC) for providing the geometry of the ELSY primary coolant system used in the simulations.

References

- [1] U.S. DOE Nuclear Energy Research Advisory Committee and The Generation IV International Forum, "A Technology Roadmap for Generation IV Nuclear Energy Systems," GIF-002-00, Dec. 2002.
- [2] V. Sobolev, "Database of thermophysical properties of liquid metal coolants for GEN-IV," SCK•CEN-BLG-1069, 2011.
- [3] V. I. Subbotin, M. N. Arnol'dov, F. A. Kozlov, and A. L. Shimkevich, "Liquid-metal coolants for nuclear power," *At. Energy*, vol. 92, no. 1, pp. 29–40, 2002.
- [4] OECD/NEA Nuclear Science Committee, "Handbook on Lead-bismuth Eutectic Alloy and Lead Properties, Materials Compatibility, Thermal-hydraulics and Technologies," 2015.
- [5] H. U. Wider, J. Carlsson, and E. Loewen, "Renewed interest in lead cooled fast reactors," *Prog. Nucl. Energy*, vol. 47, no. 1–4, pp. 44–52, Jan. 2005.
- [6] B. W. Spencer, "The rush to heavy liquid metal reactor coolants – gimmick or reasoned," in *Proc. of the 8th International Conference on Nuclear Engineering (ICONE-8)*, 2000.
- [7] E. P. Loewen and A. T. Tokuhiko, "Status of Research and Development of the Lead-Alloy-Cooled Fast Reactor," *J. Nucl. Sci. Technol.*, vol. 40, no. 8, pp. 614–627, Aug. 2003.
- [8] F. Roelofs, A. Shams, J. Pacio, V. Moreau, P. Planquart, K. Van Tichelen, I. Di Piazza,

- and M. Tarantino, “European outlook for LMFR thermal hydraulics,” in *NURETH-16*, 2015.
- [9] P. Kudinov and T. Dinh, “Evaluation approach and case set-up for simulation of consequences of the SGTR event,” ELSY project deliverable DEL/09/29, 2010.
- [10] P. E. MacDonald, V. N. Shah, L. W. Ward, and P. G. Ellison, “Steam generator tube failures,” NUREG/CR-6365, INEL-95/0383, 1996.
- [11] D. R. Diercks, W. J. Shack, and J. Muscara, “Overview of steam generator tube degradation and integrity issues,” *Nucl. Eng. Des.*, vol. 194, no. 1, pp. 19–30, Nov. 1999.
- [12] Nuclear Energy Institute, “Steam Generator Program Guideline,” NEI 97-06 (Rev. 3), 2011.
- [13] T. B. Cochran, H. A. Feiveson, W. Patterson, G. Pshakin, M. V Ramana, M. Schneider, T. Suzuki, and F. von Hippel, “Fast breeder reactor programs: history and status,” *Int. Panel Fissile Mater.*, 2010.
- [14] G. Forasassi and R. Lo Frano, “Steam Generator Tube Rupture (SGTR) preliminary analysis applied to the ELSY reactor,” Pisa, 2009.
- [15] S. Wang, M. Flad, and W. Maschek, “Evaluation of a steam generator tube rupture accident in an accelerator driven system with lead cooling,” *Prog. Nucl. ...*, vol. 50, no. 2–6, pp. 363–369, Mar. 2008.
- [16] A. Del Nevo, A. Ciampichetti, M. Tarantino, L. Burgazzi, and N. Forgiione, “Addressing the heavy liquid metal – Water interaction issue in LBE system,” *Prog. Nucl. Energy*, vol. 89, pp. 204–212, 2016.
- [17] A. Ciampichetti, D. Pellini, and P. Agostini, “Experimental and computational investigation of LBE–water interaction in LIFUS 5 facility,” ... *Eng. Des.*, vol. 239, no. 11, pp. 2468–2478, Nov. 2009.
- [18] Y. Sibamoto, Y. Kukita, and H. Nakamura, “Simultaneous measurement of fluid temperature and phase during water jet injection into high temperature melt,” in *The 11th International Topical Meeting on Nuclear Thermal-Hydraulics (NURETH-11)*, 2005, no. 181.
- [19] S. J. Board, R. W. Hall, and R. S. Hall, “Detonation of fuel coolant explosions,” *Nature*, vol. 254, pp. 319–321, 1975.
- [20] B. F. Gromov, O. G. Grigoriev, A. V Dedoul, A. V Zrodnikov, G. I. Toshinsky, and V. I. Chitaikin, “Use of Russian Technology of Ship Reactors with Lead-bismuth Coolant in Nuclear Power,” in *Based on authors’ reports of the Conference on Heavy Liquid Metal Coolants in Nuclear Technologies (HLMC-98)*, 1999.
- [21] C. Döderlein, K. Tucek, J. Cetnar, P. Stanisz, G. Grasso, and A. Travleev, “Definition of the ELFR Core and Neutronic Characterization,” LEADER project deliverable DEL005-2011, 2013.
- [22] M. Sarotto, C. Artioli, G. Grasso, D. Gugiu, and A. Travleev, “ELSY core design static, dynamic and safety parameters with the open square FA,” ELSY project deliverable DEL/09/008, 2009.
- [23] K. Tucek, K. Mikityuk, F. Manni, D. Gugiu, J. Cetnar, and G. Grasso, “ELFR cores. Summary, synoptic tables, conclusions and recommendations,” LEADER project deliverable DEL-028-2013, 2013.

- [24] C. Petrovich, G. Grasso, P. Sciora, C. Artioli, and F. Rocchi, “Definition of the ETDR Core and Neutronic Characterization,” LEADER project deliverable DEL007-2012, 2013.
- [25] S. Bortot and C. Artioli, “Investigation of the void reactivity effect in large-size Lead Fast Reactors,” *Ann. Nucl. Energy*, vol. 38, no. 5, pp. 1004–1013, 2011.
- [26] M. Eriksson, J. Wallenius, M. Jolkkonen, and J. E. Cahalan, “Inherent safety of fuels for accelerator-driven systems,” *Nucl. Technol.*, vol. 151, no. 3, pp. 314–333, 2005.
- [27] J. Carlsson, *Inherent Safety Features and Passive Prevention Approaches for Pb / Bi-cooled Accelerator-Driven Systems*. 2003.
- [28] P. Wolniewicz, A. Håkansson, P. Jansson, and S. J. Svärd, “Feasibility study of detection of coolant void in liquid metal cooled fast reactors using changes in the neutron spectrum,” *Nucl. Eng. Des.*, vol. 265, pp. 1255–1265, Dec. 2013.
- [29] P. Wolniewicz, C. Hellesen, A. Håkansson, S. J. Svärd, P. Jansson, and M. Österlund, “Detecting neutron spectrum perturbations due to coolant density changes in a small lead-cooled fast nuclear reactor,” *Ann. Nucl. Energy*, vol. 58, pp. 102–109, Aug. 2013.
- [30] M. Frogheri, “Safety Approach for LFR Plants,” LEADER project deliverable DEL-004-2011, 2011.
- [31] M. Reale, “Reactor Assembly Configuration Report And Drawings,” ELSY project deliverable DEL/11/020, 2011.
- [32] A. Alemberti, J. Carlsson, E. Malambu, A. Orden, D. Struwe, P. Agostini, and S. Monti, “European lead fast reactor—ELSY,” *Nucl. Eng. Des.*, vol. 241, no. 9, pp. 3470–3480, Sep. 2011.
- [33] L. Cinotti, “Nuclear reactor with compact primary heat exchanger,” 26-Jun-2013.
- [34] D. de Lorenzo, “Report of MS & FW System Capability and Functionality,” ELSY project deliverable DEL/07/019, 2007.
- [35] W. Xu, Q. Chen, and F. T. M. Nieuwstadt, “A new turbulence model for near-wall natural convection,” *Int. J. Heat Mass Transf.*, vol. 41, no. 21, pp. 3161–3176, Nov. 1998.
- [36] L. Cinotti, “Reactor Assembly Preliminary Configuration,” ELSY project deliverable DOC/08/049, 2008.
- [37] A. Onea, M. Böttcher, and D. Struwe, “Lead pressure loss in the heat exchanger of the ELSY fast lead-cooled reactor by CFD approach,” in *Benchmarking of CFD Codes for Application to Nuclear Reactor Safety (CFD4NRS-3)*, 2010.
- [38] A. A. Kulkarni and J. B. Joshi, “Bubble Formation and Bubble Rise Velocity in Gas - Liquid Systems : A Review,” pp. 5873–5931, 2005.
- [39] R. Clift, J. R. Grace, and M. E. Weber, *Bubbles, drops, and particles*. Courier Corporation, 2005.
- [40] G. Q. Yang, B. Du, and L. S. Fan, “Bubble formation and dynamics in gas–liquid–solid fluidization—A review,” *Chem. Eng. Sci.*, vol. 62, no. 1–2, pp. 2–27, Jan. 2007.
- [41] J. O. Hinze, “Fundamentals of the hydrodynamic mechanism of splitting in dispersion processes,” *AIChE J.*, vol. 1, no. 3, pp. 289–295, 1955.
- [42] G. M. Evans, G. J. Jameson, and B. W. Atkinson, “Prediction of the Bubble Size

- Generated by a Plunging Liquid Jet Bubble Column,” *Chem. Eng. Sci.*, vol. 47, no. 13/14, pp. 3265–3272, 1992.
- [43] K. Terasaka, Y. Sasada, and D. Kobayashi, “Submilli-Bubble Dispersion from a Slit Orifice into Water,” vol. 44, no. 3, pp. 140–145, 2011.
- [44] A. V. Beznosov, S. S. Pinaev, D. V. Davydov, A. A. Molodtsov, T. A. Bokova, P. N. Martynov, and V. I. Rachkov, “Experimental Studies of the Characteristics of Contact Heat Exchange Between Lead Coolant and the Working Body,” *At. Energy*, vol. 98, no. 3, pp. 170–176, Mar. 2005.
- [45] Y. Xie, S. Orsten, and F. Oeters, “Behaviour of Bubbles at Gas Blowing into Liquid Wood’s Metal,” *ISIJ Int.*, vol. 32, no. 1, pp. 66–75, 1992.
- [46] H. D. Mendelson, “The Prediction of Bubble Terminal Rise Velocities from Wave Theory,” *AIChE J.*, vol. 13, no. 2, pp. 250–253, 1967.
- [47] M. Jamialahmadi, C. Branch, and H. Müller-Steinhagen, “Terminal bubble rise velocity in liquids,” *Chem. Eng. Res. Des.*, vol. 72, no. 1, pp. 119–122, 1994.
- [48] K. Schwerdtfeger, “Velocity of rise of argon bubbles in mercury,” *Chem. Eng. Sci.*, vol. 23, no. 8, pp. 937–938, Aug. 1968.
- [49] Y. Mori, K. Hijikata, and I. Kuriyama, “Experimental Study of Bubble Motion in Mercury With and Without a Magnetic Field,” *J. Heat Transfer*, vol. 99, no. 3, pp. 404–410, Aug. 1977.
- [50] C. Zhang, S. Eckert, and G. Gerbeth, “Experimental study of single bubble motion in a liquid metal column exposed to a DC magnetic field,” *Int. J. Multiph. Flow*, vol. 31, no. 7, pp. 824–842, Jul. 2005.
- [51] J. Szekely, *Fluid Flow Phenomena in Metals Processing*. Elsevier, 1979.
- [52] L. Schiller and A. Naumann, “Über die grundlegenden Berechnungen bei der Schwerkraftaufbereitung,” *Z. Ver. Dtsch. Ing.*, vol. 77, no. 12, pp. 318–320, 1933.
- [53] D. Rodrigue, “Generalized correlation for bubble motion,” *AIChE J.*, vol. 47, no. 1, pp. 39–44, Jan. 2001.
- [54] D. Rodrigue, “Drag coefficient—reynolds number transition for gas bubbles rising steadily in viscous fluids,” *Can. J. Chem. Eng.*, vol. 79, no. 1, pp. 119–123, Feb. 2001.
- [55] G. Bozzano and M. Dente, “Single bubble and drop motion modeling,” in *Chemical Engineering Transactions*, 2009, vol. 17, pp. 567–572.
- [56] A. Tomiyama, I. Kataoka, I. Zun, and T. Sakaguchi, “Drag Coefficients of Single Bubbles under Normal and Micro Gravity Conditions,” *JSME Int. journal. Ser. B, Fluids Therm. Eng.*, vol. 41, no. 2, pp. 472–479, May 1998.
- [57] K. Aoto, P. Dufour, Y. Hongyi, J. P. Glatz, Y. Il Kim, Y. Ashurko, R. Hill, and N. Uto, “A summary of sodium-cooled fast reactor development,” *Prog. Nucl. Energy*, vol. 77, pp. 247–265, 2014.
- [58] B. Flesch and B. Cochet, “Leak-before-break in steam generator tubes,” *Int. J. Press. Vessel. Pip.*, vol. 43, no. 1–3, pp. 165–179, Jan. 1990.
- [59] S. S. Hwang, H. P. Kim, J. S. Kim, K. E. Kasza, J. Park, and W. J. Shack, “Leak behavior of SCC degraded steam generator tubings of nuclear power plant,” *Nucl. Eng. Des.*, vol. 235, no. 23, pp. 2477–2484, Dec. 2005.